J. Fluid Mech. (2011), *vol.* 672, *pp.* 411–427.
doi:10.1017/S0022112010006099

Mechanism of drag reduction by a surface trip wire on a sphere

KWANGMIN SON[1], JIN CHOI[1], WOO-PYUNG JEON[1] AND HAECHEON CHOI[1,2]†

[1]School of Mechanical and Aerospace Engineering, Seoul National University, Seoul 151-744, Korea
[2]Institute of Advanced Machinery and Design, Seoul National University, Seoul 151-744, Korea

(Received 10 May 2010; revised 12 November 2010; accepted 15 November 2010; first published online 14 February 2011)

The effect of a surface trip wire on the flow around a sphere is experimentally investigated at subcritical Reynolds numbers of $Re = 0.5 \times 10^5$–2.8×10^5 based on the free-stream velocity U_∞ and sphere diameter d. By varying the streamwise location (20°–70° from the stagnation point) and diameter ($0.33 \times 10^{-2} < k/d < 1.33 \times 10^{-2}$) of a trip wire, we measure the drag, surface pressure distribution and boundary layer velocity profiles above the sphere surface, and conduct flow visualization. Depending on the size and streamwise location of the trip wire, three different flow characteristics are observed above the sphere surface. For low Reynolds numbers, the disturbance induced by the trip wire decays downstream and main separation occurs at a streamwise location similar to that of a smooth sphere. As the Reynolds number is increased, laminar separation is delayed farther downstream by the disturbance from the trip wire and the transition to turbulence occurs along the separated shear layer, resulting in the flow reattachment to the sphere surface and thus forming a secondary separation bubble on the sphere surface. Then, the main separation is delayed due to high momentum near the surface and the drag is significantly reduced. When the trip wire produces even larger disturbances through the separation and reattachment right at the trip-wire location for higher Reynolds numbers, the boundary layer flow becomes turbulent soon after the trip-wire location and the main separation is delayed, resulting in drag reduction.

Key words: drag reduction, separated flows

1. Introduction

Although the sphere is a simple three-dimensional bluff body, the flow around it shows a significant variation with the Reynolds number (Achenbach 1972). When the Reynolds number based on the free-stream velocity (U_∞) and sphere diameter (d) is $Re \approx 0.5 \times 10^5$–$2 \times 10^5$, laminar separation occurs at the azimuthal angle of $\phi \approx 80°$ and the drag coefficient is nearly constant ($C_D \approx 0.5$) regardless of the Reynolds number. In the Reynolds number range of $2 \times 10^5 < Re \lesssim 3.7 \times 10^5$, the drag coefficient rapidly decreases with the Reynolds number and reaches a minimum value ($C_D \approx 0.07$). This phenomenon is called 'drag crisis', and the Reynolds number at which the drag coefficient becomes minimum is called the critical Reynolds number. With further increase in the Reynolds number, the drag coefficient slowly increases from the minimum value. It has been shown by Fage (1936) and Suryanarayana &

† Email address for correspondence: choi@snu.ac.kr

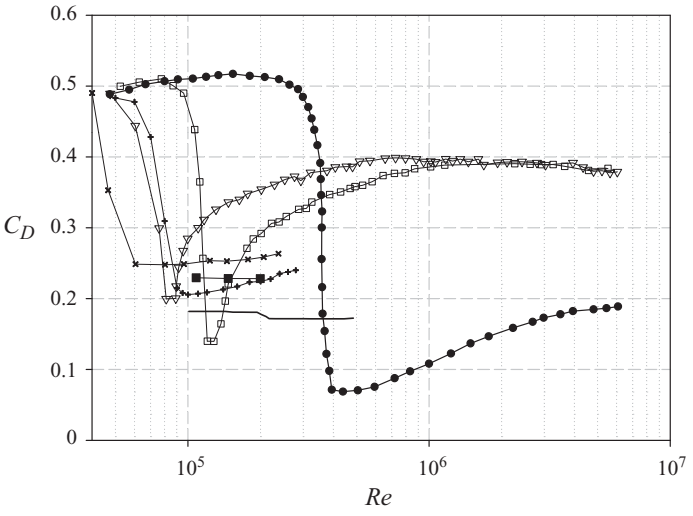

FIGURE 1. Variations of the drag coefficient with the Reynolds number for smooth, dimpled, roughened and tripped spheres: ●, smooth (Achenbach 1972); ×, dimpled ($k/d = 0.9 \times 10^{-2}$, Bearman & Harvey 1976); +, dimpled ($k/d = 0.4 \times 10^{-2}$, Choi, Jeon & Choi 2006); ▽, roughened ($k/d = 1.25 \times 10^{-2}$, Achenbach 1974); □, roughened ($k/d = 0.5 \times 10^{-2}$, Achenbach 1974); ■, tripped ($k/d = 0.33 \times 10^{-2}$, Maxworthy 1969); ———, tripped (k/d not available, Wieselsberger 1914). Here, k is the height of roughness, diameter of trip wire or depth of dimples.

Prabhu (2000) that at the critical Reynolds number the flow separated from a laminar boundary layer at $80^\circ < \phi < 110^\circ$ reattaches to the sphere surface at $\phi \approx 110^\circ$ (and thus forming a secondary separation bubble on the sphere surface) and delays main separation, which is the key mechanism responsible for the drag-crisis phenomenon.

So far, many different control strategies for the reduction of drag on the sphere in a uniform flow have been suggested (see Choi, Jeon & Kim 2008 for a review) such as the surface roughness (Achenbach 1974), dimples (Bearman & Harvey 1976; Choi *et al.* 2006; Smith *et al.* 2009), surface trip wire (Wieselsberger 1914; Maxworthy 1969), free-stream disturbance (Raithby & Eckert 1968; Moradian, Ting & Cheng 2009; Son *et al.* 2010) and periodic blowing and suction (Jeon *et al.* 2004). Some of the previous control results are given in figure 1. Among them, some controls such as the dimples, periodic blowing and suction and free-stream disturbance share the same drag-reduction mechanism as that of drag-crisis phenomenon. That is, owing to the control, the shear layer separated from a laminar boundary layer undergoes transition to turbulence that brings high momentum towards the sphere surface, and the flow reattaches and becomes a turbulent boundary layer that delays the main separation. When this happens ('modified' drag crisis), the drag coefficient is rapidly decreased and reaches a minimum value. An interesting feature is that this minimum drag coefficient is nearly unchanged even at higher Reynolds numbers (see, for example C_D of dimples in figure 1).

Unlike those controls, the surface roughness has a different drag-reduction mechanism (Achenbach 1974). In this case, the laminar boundary layer is directly triggered by the surface roughness and changed into a turbulent boundary layer through transition. Then, the main separation is delayed due to high momentum near the surface and drag reduction occurs. One interesting feature is that the drag

coefficient becomes minimum at 'modified' critical Reynolds number and then rapidly increases with the Reynolds number. The increase in the drag coefficient after the modified critical Reynolds number comes from the upstream shift of separation line due to earlier growth of turbulent boundary layer by the surface roughness at higher Reynolds number. A common feature of dimples and roughness from figure 1 is that both the modified critical Reynolds number and the amount of drag reduction decrease with increasing k (roughness height or dimple depth). This is because a higher k produces sufficient disturbances for transition to turbulence at an earlier streamwise surface location even in the case of lower Reynolds number.

The observation of the $C_D - Re$ data for the surface trip wire (Wieselsberger 1914; Maxworthy 1969) in figure 1 suggests that the mechanism responsible for the drag reduction by the surface trip wire should be similar to that of dimples rather than that of surface roughness, because the reduced C_D values are nearly constant. On the other hand, unlike the dimples and roughness, the surface trip wire generates two-dimensional local disturbances. Therefore, the mechanism responsible for drag reduction by the surface trip wire may be different from those of dimples and surface roughness.

There have been only a few studies on the flow around a sphere with a surface trip wire. Wieselsberger (1914) conducted the first experiment on this flow and showed a significant drag reduction with a surface trip wire. Maxworthy (1969) attached a trip wire of $k/d = 0.33 \times 10^{-2}$ on a sphere at $\phi = 55^\circ$ to induce turbulent boundary layer separation at subcritical Reynolds numbers. As a result, the flow separation was delayed to occur at $\phi = 100^\circ$–110° and the drag coefficient obtained by the integration of the surface pressure was significantly reduced ($C_D = 0.23$). Oil-flow visualization and surface pressure distribution also indicated that direct transition to turbulence occurred at the trip-wire location as was intended. However, the reduced drag coefficient in the presence of a surface trip wire showed a considerable difference from that of Wieselsberger (1914), although there was no information about the size and location of the trip wire used by Wieselsberger (1914). Recently, Bakić (2004) conducted a laser-Doppler anemometry (LDA) experiment for a sphere with a trip wire of $k/d = 0.81 \times 10^{-2}$ located at $\phi = 75^\circ$ ($Re = 51,500$), and showed that the separation was delayed to $\phi = 120^\circ$ and the size of the recirculation zone in the wake was decreased. Torlak *et al.* (2004) conducted a large eddy simulation (LES) for the same geometry as in Bakić (2004). However, their mean flow parameters such as the separation point and the size of recirculation region were notably different from the experimental ones.

The surface trip wire has also been applied to the flow over a circular cylinder (Zdravkovich 1997). Fage & Warsap (1929) attached a pair of trip wires at $\phi = \pm 65^\circ$ on the upper and lower cylinder surfaces, respectively, by varying the diameter of trip wires ($0.02 \times 10^{-2} < k/d < 0.3 \times 10^{-2}$; smaller than local boundary layer thickness) for $0.9 \times 10^5 < Re < 2.62 \times 10^5$. They found that the drag coefficient is reduced at lower Reynolds number with increasing trip-wire diameter. James & Truong (1972) attached a single trip wire of $0.6 \times 10^{-2} < k/d < 6.3 \times 10^{-2}$ at $\phi = 15^\circ$– 90° for $10^4 < Re < 10^5$. The trip wires located at $\phi = 45^\circ$– 70° produced significant drag reductions, but those at other azimuthal angles showed nearly no drag reduction. Fujita, Takahama & Kawai (1985) studied the effect of surface trip wire on heat transfer, evaluated by the measurement of the surface pressure distribution. A pair of trip wires of $0.2 \times 10^{-2} < k/d < 4 \times 10^{-2}$ were attached at $\phi = 15^\circ$–90°. They classified the heat-transfer distributions into three patterns (see below), although clear criteria for these classifications were not given. Igarashi (1986) conducted flow visualizations and

measured the surface pressure distributions at various Reynolds numbers for different trip-wire sizes and locations. As a result, three distinct flow patterns near the trip-wire location were reported: (i) relaminarization after the trip wire, (ii) formation of turbulent boundary layer flow and (iii) full separation at the trip-wire location. Finally, Hover, Tvedt & Triantafyllou (2001) studied the effect of a surface trip wire on the flow properties in the wake, and vortex-induced load and vibration for $Re \leqslant 4.6 \times 10^4$. They showed that the mean drag and lift fluctuations are significantly reduced and the Strouhal number is increased to a value around $St = fd/U_\infty = 0.25$–0.27, where f is the vortex shedding frequency.

Apart from its application to bluff bodies such as the sphere and circular cylinder, the surface trip wire has been widely used as a passive control device for other various geometries such as aerofoils (Carmichael 1981; Lissaman 1983; Lyon, Selig & Broeren 1997; Gopalarathnam *et al.* 2003) and turbine blades (Volino 2003; Zhang & Hodson 2005). For example, the surface trip wire has been used to improve the performance of low-Reynolds-number ($10^4 < Re < 10^6$) aerofoils by eliminating or reducing laminar separation bubble existing on the aerofoil surface (see Gal-el-Hak 1990 for a comprehensive review on this topic). For these aerofoils, separation, transition and reattachment could all occur on the aerofoil surface, thus forming a laminar separation bubble and affecting their aerodynamic performance. Since turbulent flow is usually more resistant to separation, promoting transition from laminar to turbulent boundary layer through a surface trip wire can be quite effective in certain conditions. For an aerofoil having a long separation bubble (20 %–30 % of the chord length), the application of surface trip wire typically induces a large drag reduction. However, it is rather ineffective for an aerofoil having a small separation bubble (an order of a few per cent of the chord length) due to added device drag caused by the protuberance effect together with an increased skin friction. Lyon *et al.* (1997) and Gopalarathnam *et al.* (2003) performed systematic experimental investigations and suggested that (i) small two-dimensional surface trips produce large drag reduction, (ii) the location of surface trip has little effect on the drag as long as it is positioned upstream of the laminar separation and (iii) aerofoils designed with surface trip wires are unable to achieve better drag performance than an untripped aerofoil having a small bubble. Hence, the strategy of applying the surface trip to a streamlined body may be very different from that to a bluff body because in the latter case the surface trip should modify massive flow separation.

As described above, many studies have shown that the surface trip wire can significantly reduce the drag forces on bluff bodies such as the cylinder and sphere and streamlined bodies such as the aerofoil. However, only a few studies have investigated the mechanism responsible for the drag reduction by the surface trip wire on the sphere and two-dimensional cylinder. So far, it has been shown that direct transition to turbulence in a boundary layer flow before separation is the main cause of drag reduction by the trip wire. However, this does not clearly explain why the drag coefficient remains constant after the modified critical Reynolds number as shown in figure 1 (Wieselsberger 1914; Maxworthy 1969). So, there should be some other important flow phenomenon near the trip wire which may be associated with the drag reduction. Therefore, the objective of the present study is to investigate the mechanism of drag reduction by the surface trip wire for flow around a sphere at subcritical Reynolds numbers of $Re = 0.5 \times 10^5$–2.8×10^5. We vary the diameter ($k/d = 0.33 \times 10^{-2}, 0.67 \times 10^{-2}$ and 1.33×10^{-2}) and streamwise location ($\phi = 20°$–$70°$) of the surface trip wire. We measure the drag, surface pressure distribution and streamwise velocity profiles above the sphere surface, and conduct

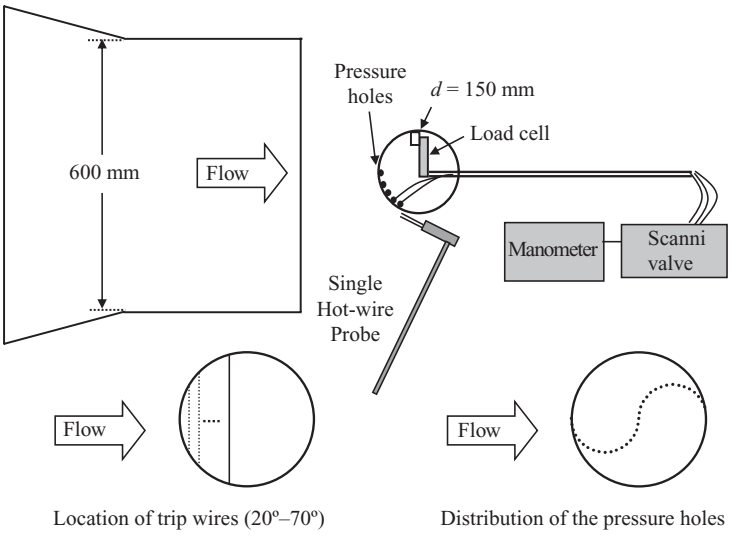

FIGURE 2. Schematic diagram of the experimental setup.

surface flow visualization. The mechanism of drag reduction and the change in the flow characteristics near the sphere surface are provided in this study.

2. Experimental setup

Figure 2 shows the schematic diagram of the present experimental setup, which is nearly the same as that used in our previous experiment (Son *et al.* 2010). The experiment is conducted in an open-circuit blowing-type wind tunnel having the test section of 600 mm × 600 mm made of acryl. The maximum wind speed at the test section is 30 m s^{-1} and the uniformities of mean velocity and background turbulence intensity at 10 m s^{-1} are within 0.7 % and 0.5 %, respectively. Our previous experimental study on the effect of free-stream turbulence (Son *et al.* 2010) showed that the background turbulence intensity within 0.5 % is low and has little influence on the flow characteristics at the Reynolds number range investigated in the present study. The sphere of 150 mm in diameter is made of ABS resin. The blockage ratio of the cross-sectional area of sphere to the test-section area is about 5 %, which is below the critical value ensuring negligible blockage effect on the flow field according to Achenbach (1974). The sphere is supported at the rear by a steel rod of 19 mm in diameter and 1000 mm in length. To prevent the sphere from vibration, the steel rod (supporter) is tightly fixed to a heavy steel frame that consists of 12 edges of a rectangular parallelepiped and is anchored to the ground. For the measurement of the velocity above the sphere surface, four suspension wires (diameter of 1.0 mm) attached to the sphere surface at the azimuthal angle of $\phi = 130^\circ$ are additionally fastened to the steel frame. The data from the measurement are transferred to a computer through an A/D converter (NI-7409) and post-processed.

The range of the Reynolds number for the present experiment is $Re = 0.5 \times 10^5$–2.8×10^5. Three different surface trip wires of 0.5, 1.0 and 2.0 mm in diameter (k) are used and the location of each trip wire varies from $\phi = 20^\circ$ to 70° by increments of 10°. The drag on the sphere is measured directly using a load cell (CASS BCL-1L). The suspension wires are detached in this case because the force on

the sphere is changed in their presence. The magnitude of drag is small (0.25–4 N) and sensitive to external interferences, so the load cell is directly installed inside the sphere (figure 2) and calibrated every time before measurement. Here, the load cell is fixed to the supporter and the sphere is connected to the load cell by two screws without touching the supporter for an accurate force measurement. The calibration curve is linear and the uncertainty of drag measurement is $\pm 2.5\,\%$ at $Re = 0.5 \times 10^5$ and $\pm 1.0\,\%$ at $Re = 2.0 \times 10^5$. The output from the load cell is amplified and sampled for 30 s at the rate of 32 kHz to obtain the mean drag. The surface-pressure distribution in the azimuthal direction (ϕ) is measured through 27 taps with a scannivalve and a pressure transducer (MKS 220DD). The taps are drilled normal to the surface in a spiral shape to avoid interference between the pressure ports (figure 2). The resolution of the pressure transducer is 0.001 % at full scale of 10 Torr and the output signal is sampled for 15 s at the rate of 100 Hz. The pressure distribution along the surface of the smooth sphere (i.e. without trip wire) at a subcritical Reynolds number shows good agreement with those from the previous experimental studies (Fage 1936; Achenbach 1972; Jeon *et al.* 2004). The drag coefficient obtained from the integration of the surface pressure of the smooth sphere is about 5 % lower than that from direct load-cell measurement; this difference comes from the skin-friction drag. Surface visualizations are conducted using a mixture of oil and titanium dioxide and the oil-flow patterns are photographed from the top of the sphere because the oil movement is influenced by gravity on the side and bottom surfaces of the sphere.

The boundary layer velocity profiles are measured with an in-house multi-channel hot-wire anemometer and a single hot-wire probe. The sensor used is a platinum-10 % rhodium wire with a diameter of 2.5 μm and a length of 0.5 mm that is soldered to the prongs. At an overheat ratio of 1.2, the cutoff frequency of the sensor is approximately 30 kHz. The voltages from the anemometer are calibrated at the free-stream with a standard two-hole Pitot tube and a digital manometer. A polynomial of fourth order is used to form a least-square fit of the voltage versus the velocity. The uncertainty in the velocity measurement is within $\pm 0.5\,\%$ immediately after calibration, and when the sensor drifts by more than 2 % after each measurement, data is rejected and the calibration process is repeated. The output from the hot-wire sensor is sampled for 15 s at the rate of 32 kHz. The hot-wire probe is positioned in the flow by a two-dimensional traversing unit (resolution is 0.02 mm) that is controlled automatically using a computer and a stepping motor. When the hot wire breaks due to the contact of the probe on the surface, we set that distance from the surface to be 0 and calculate wall-normal distances of other measurement points. Thus, the distance of the measurement location closest to the surface is 0.02 mm.

3. Results and discussion

3.1. *Drag variation*

Figure 3 shows the variations of drag coefficient with the Reynolds number for the trip wires of 0.5 mm ($k/d = 0.33 \times 10^{-2}$) and 1.0 mm ($k/d = 0.67 \times 10^{-2}$) diameters located at the azimuthal locations of $\phi = 20^\circ$–70°. Note that the boundary layer thickness at $\phi = 80^\circ$ above the smooth sphere is 0.68 mm for $Re = 10^5$. The drag coefficient of the smooth sphere is around 0.5 at the Reynolds numbers considered (figure 3), which agrees well with the results of Achenbach (1972) shown in figure 1. As the trip wire locates farther downstream, the drag coefficient starts to decrease at lower Reynolds number and the modified critical Reynolds number (Re_c) also decreases. However, the drag coefficient remains nearly constant ($C_D \approx 0.18$) for $Re \geqslant Re_c$ irrespective of

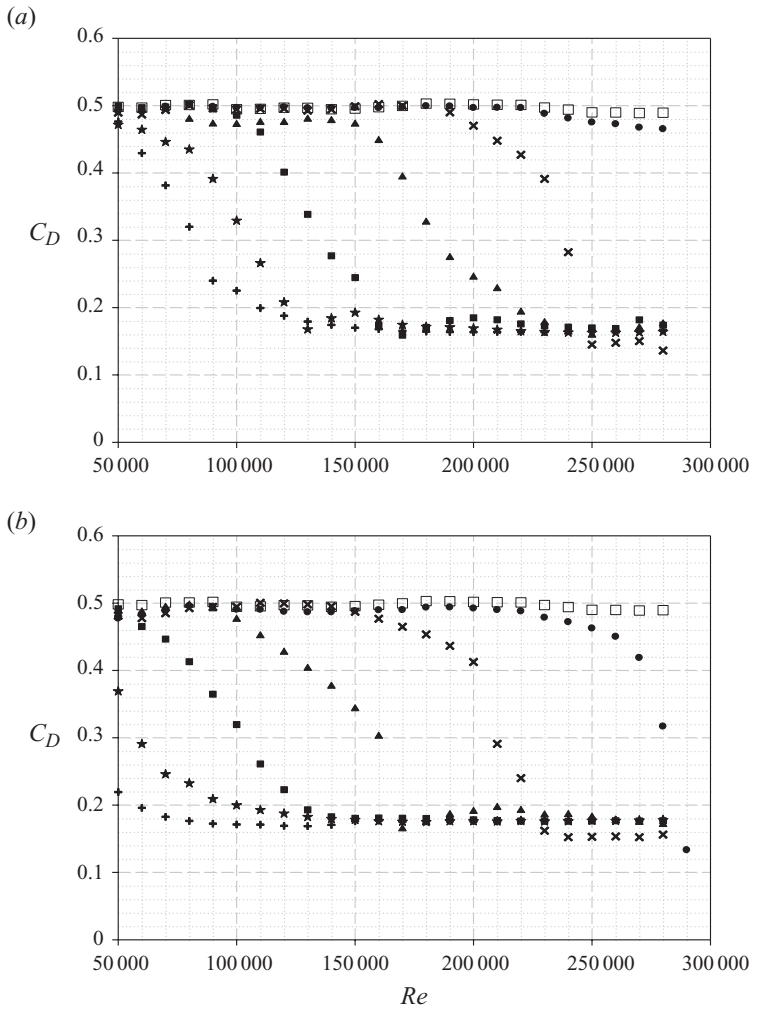

FIGURE 3. Variations of the drag coefficient with the Reynolds number: (*a*) $k/d = 0.33 \times 10^{-2}$; (*b*) 0.67×10^{-2}. □, Smooth sphere; ●, $\phi = 20°$; ×, 30°; ▲, 40°; ■, 50°; ★, 60°; +, 70°. Here, ϕ is the location of the trip wire.

the trip-wire location. The amount of drag reduction is more than 60 % for $Re \geqslant Re_c$ as compared to that of a smooth sphere before it reaches its own Re_c. Note also that the bigger size of the trip wire produces an earlier decrease in the drag coefficient and smaller Re_c. It is interesting to see that the behaviour of the C_D–Re curve for the trip wire is similar to that of dimples rather than that of roughness, in that C_D is nearly constant after modified critical Reynolds number. However, in the case of dimples, the magnitude of C_D for $Re \geqslant Re_c$ increases with increasing k/d, whereas it increases slightly with k/d as shown in figures 3 and 4 (see below).

Figure 4 shows the variations of the drag coefficient with the Reynolds number for three different sizes of trip wires ($k/d = 0.33 \times 10^{-2}$, 0.67×10^{-2} and 1.33×10^{-2}) located at $\phi = 50°$. As shown, the modified critical Reynolds number decreases with increasing trip-wire diameter because larger disturbances promote earlier transition to turbulence (see § 3.4). As mentioned before, the drag coefficient for $Re \geqslant Re_c$ is

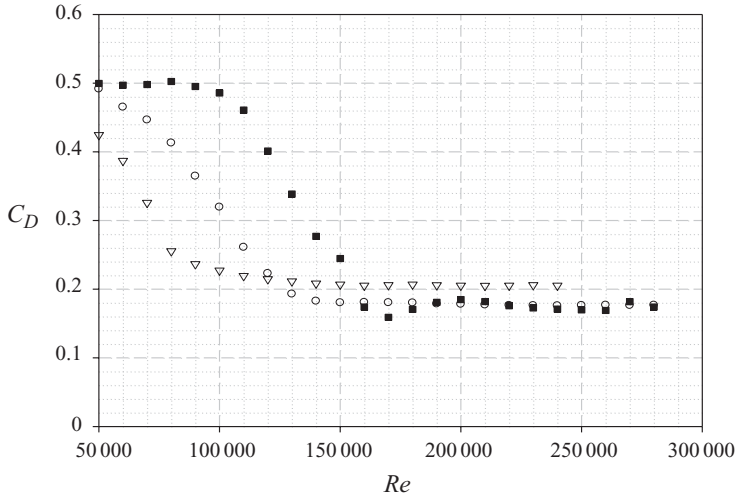

FIGURE 4. Variations of the drag coefficient with the Reynolds number for three different diameters of trip wires located at $\phi = 50°$: ■, $k/d = 0.33 \times 10^{-2}$; ○, 0.67×10^{-2}; ▽, 1.33×10^{-2}.

almost constant irrespective of the Reynolds number and the diameter of trip wire, although there is a slight increase in the drag coefficient with increasing k/d.

3.2. *Surface flow visualization*

Figure 5 shows the surface oil-flow patterns at various Reynolds numbers for the trip wires of $k/d = 0.33 \times 10^{-2}$ and 1.33×10^{-2} located at $\phi = 50°$. Oil is moved by the wall shear stress and is accumulated near the location of zero shear stress where flow separation occurs. For a smooth sphere ($C_D = 0.5$), oil is accumulated around $\phi \approx 80°$ in the subcritical Reynolds number range (not shown here). With the trip wire of $k/d = 0.33 \times 10^{-2}$ located at $\phi = 50°$ (figure 5*a*), the separation point for $Re = 0.7 \times 10^5$ is similar to that of a smooth sphere. As the Reynolds number increases, the separation is gradually delayed downstream. At $Re = 1.2 \times 10^5$, the separation occurs at $\phi \approx 90°$ and the drag is reduced by 20 % ($C_D = 0.4$ in figure 4). Near the modified critical Reynolds number ($Re_c = 1.5 \sim 1.7 \times 10^5$; figure 4), three conspicuous lines appear on the rear part of the sphere surface due to the trip wire. These lines correspond to the lines of laminar separation, reattachment and turbulent separation, respectively. A secondary separation bubble, which is a closed-loop streamline from laminar separation to reattachment, exists on the sphere surface and delays the main separation to a farther downstream location. Interestingly, as the Reynolds number further increases, the laminar separation is delayed farther downstream but the reattachment line closing the separation bubble is fixed around $\phi = 110°$, thus decreasing the size of the secondary separation bubble with increasing Reynolds number. The main separation line is also fixed at $\phi = 120°$–$130°$, which results in a nearly constant drag coefficient for $Re \geqslant Re_c$. The secondary separation bubble finally disappears at $Re = 2.3 \times 10^5$, but the location of main separation is unchanged, maintaining nearly constant drag coefficient ($C_D \approx 0.18$). Therefore, the formation of a secondary separation bubble on the sphere surface is the main cause of the rapid decrease in the drag coefficient for the trip wire of $k/d = 0.33 \times 10^{-2}$ located at $\phi = 50°$.

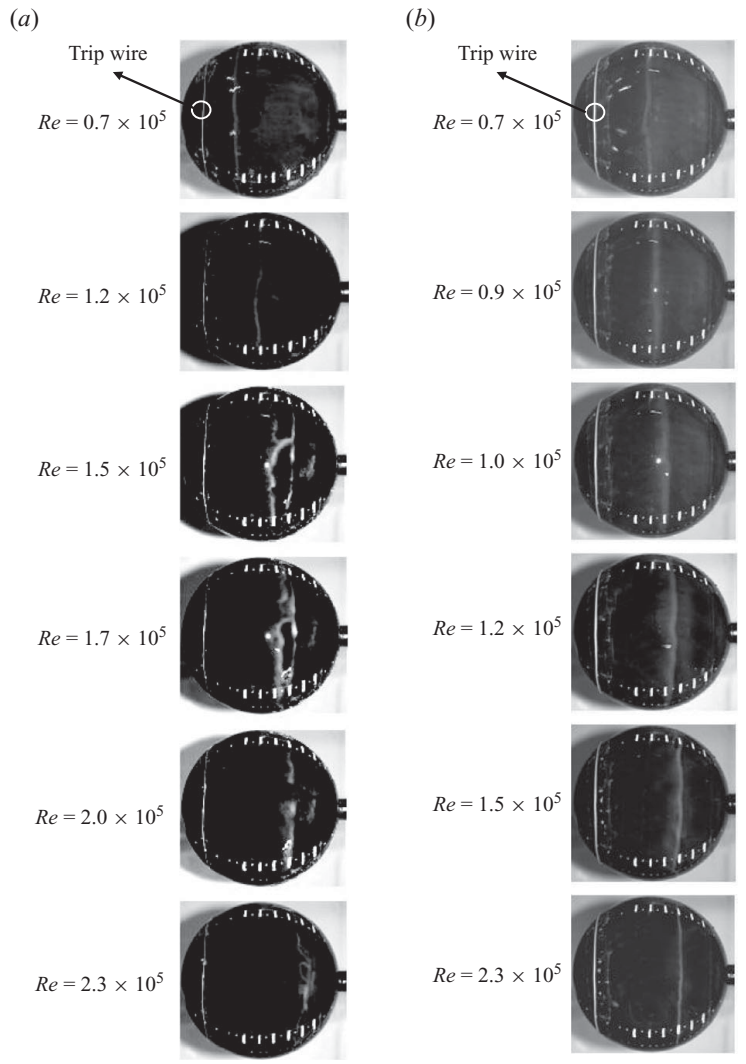

FIGURE 5. Oil-flow patterns on the sphere surface with the trip wire located at $\phi = 50°$: (*a*) $k/d = 0.33 \times 10^{-2}$; (*b*) 1.33×10^{-2}.

Now, for a larger size of trip wire ($k/d = 1.33 \times 10^{-2}$), a different drag-reduction process takes place as shown in figure 5(*b*). That is, as the Reynolds number increases, the main separation is gradually delayed farther downstream without formation of a secondary separation bubble on the rear surface and is finally fixed at $\phi \approx 110°$ for $Re \geqslant Re_c$. The trip wire under consideration is very big in size and thus it is felt as a kind of fence to the incoming boundary layer flow. Hence, unlike the smaller size of trip wire, a large recirculation zone is formed right behind the trip wire. After reattachment, turbulent boundary layer flow develops and delays the main separation. Note that the locations of main separation for the two different sizes of trip wires ($k/d = 0.33 \times 10^{-2}$ and 1.33×10^{-2}) are around 120°– 130° and 110°, respectively. Therefore, the drag coefficient after the modified critical Reynolds number is slightly smaller for the trip wire of $k/d = 0.33 \times 10^{-2}$ than for that of $k/d = 1.33 \times 10^{-2}$.

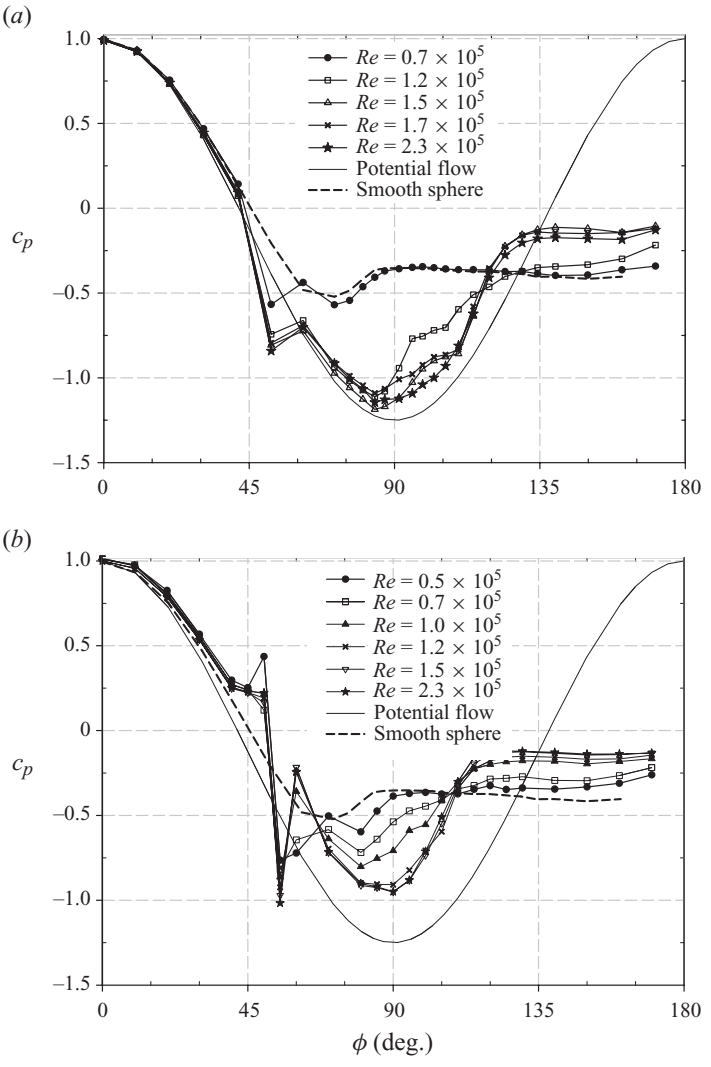

FIGURE 6. Variations of the surface pressure for the trip wires located at $\phi = 50°$: (*a*) $k/d = 0.33 \times 10^{-2}$; (*b*) 1.33×10^{-2}.

3.3. *Pressure distribution*

Figure 6 shows the variations of surface pressure with the Reynolds number for the trip wires of $k/d = 0.33 \times 10^{-2}$ and 1.33×10^{-2} located at $\phi = 50°$, together with the pressure distributions of potential and viscous flows over a smooth sphere. Due to the existence of the trip wire, the surface pressure near the trip-wire location shows local peaks. For the trip wire of $k/d = 0.33 \times 10^{-2}$ in figure 6(*a*), the pressure distribution at $Re = 0.7 \times 10^5$ is similar to that of a smooth sphere, where laminar separation occurs at $\phi \approx 80°$. As the Reynolds number increases, the pressure distribution approaches that of potential flow before main separation occurs, and the base pressure recovers significantly. Moreover, the pressure distributions for $Re \geqslant 1.5 \times 10^5$ nearly overlap, agreeing well with the constant drag coefficient at these Reynolds numbers (figure 4). It should be mentioned here that there exists a plateau in the pressure distribution curve around $\phi = 100°$–$110°$ at $Re = 1.5 \times 10^5$ and 1.7×10^5. This feature is very

similar to that observed in a smooth sphere around the critical Reynolds number, where a separation bubble exists above the sphere surface (Fage 1936; Suryanarayana & Prabhu 2000). However, the plateau in the pressure distribution curve disappears at $Re = 2.3 \times 10^5$, which agrees with the fact that only turbulent separation occurs without secondary separation bubble formation at this Reynolds number as observed in figure 5(*a*).

Figure 6(*b*) shows the surface-pressure distributions for the trip wire of $k/d = 1.33 \times 10^{-2}$ located at $\phi = 50°$. Due to the large recirculation zone formed right behind the trip wire, the pressure distribution is complicated near the trip wire and is not much close to that of potential flow as compared to that of the smaller trip wire. At $Re \geqslant 1.2 \times 10^5$, the pressure curves almost overlap among themselves and show significant base pressure recovery, indicating large drag reduction and constant $C_D (\approx 0.21)$ for $Re \geqslant Re_c$ (figure 4). Unlike the smaller trip wire, the local plateau in the pressure distribution curve is not clearly observable for this large trip wire. This supports the observation that, after reattachment behind the trip wire of $k/d = 1.33 \times 10^{-2}$, turbulent boundary layer grows and separates without formation of secondary separation bubble at the rear sphere surface. Note also that the surface pressure ahead of the trip wire of $k/d = 1.33 \times 10^{-2}$ is significantly higher than that of $k/d = 0.33 \times 10^{-2}$, although the pressure recovery behind the sphere is more or less the same for both cases. This pressure increase ahead of the large trip wire leads to a larger drag force than that from the smaller one (figure 4).

3.4. *Streamwise velocity measurement*

To investigate the detailed flow characteristics of transition to turbulence and main and secondary separations associated with the drag reduction by the trip wire, we measure the near-wall streamwise (wall-parallel) velocity along the radial direction perpendicular to the sphere surface at $\phi = 60°$–$120°$ with a single hot-wire probe. Figures 7 and 8 show these velocity profiles for the trip wires of $k/d = 0.33 \times 10^{-2}$ and 1.33×10^{-2} located at $\phi = 50°$, respectively. Note that, owing to the usage of a single hot-wire probe, the measured velocity does not accurately represent the streamwise velocity component near and after flow separation where the velocity vectors have relatively high incidence angles, and the measured mean velocity and r.m.s. velocity fluctuation profiles inside the separation bubble do not represent the real flow statistics. Nevertheless, the variations of the measured velocity along the radial and streamwise directions clearly provide how the flow changes near and after the flow separation (see below). The streamwise velocity signals at the radial locations where u_{rms} are maximum are Fourier-transformed to obtain their energy spectra. These radial locations are inside the boundary layer before separation but in the separated shear layer after separation. Figure 9 shows these energy spectra at some representative streamwise positions.

For the trip wire of $k/d = 0.33 \times 10^{-2}$ (figure 7), the velocity profiles at $Re = 0.7 \times 10^5$ are very similar to those of a smooth sphere (Jeon *et al.* 2004) as expected. That is, main separation occurs right after $\phi = 80°$ (note that flow separation is detected from constant near-wall mean velocity profile along the radial direction when a single hot-wire probe is used), and r.m.s. velocity fluctuations rapidly increase. Since the r.m.s. velocity fluctuations at $\phi = 60°$ and $70°$ are very weak, the disturbances generated by the trip wire rapidly decay in the downstream direction at this low Reynolds number. The energy spectra at $\phi = 80°$ and $90°$ also show very low energy levels at high frequencies (figure 9*a*), indicating that laminar separation occurs. At $Re = 1.7 \times 10^5$, where the drag coefficient reaches minimum (figure 4), the

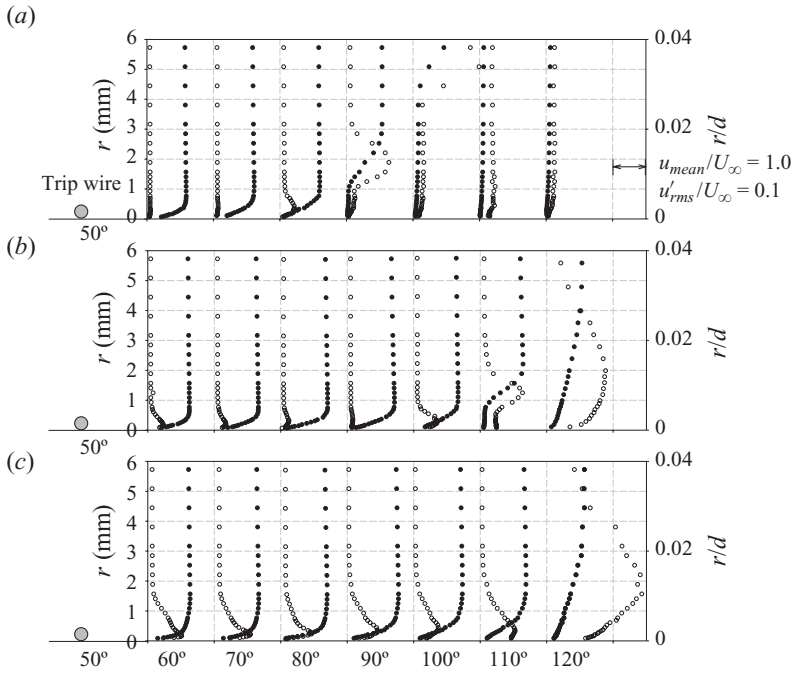

FIGURE 7. Profiles of the mean streamwise velocity (●) and r.m.s. streamwise velocity fluctuations (○) above the sphere surface at $\phi = 60°$–$120°$ for the trip wire of $k/d = 0.33 \times 10^{-2}$ located at $\phi = 50°$: (*a*) $Re = 0.7 \times 10^5$; (*b*) 1.7×10^5; (*c*) 2.3×10^5.

disturbance induced by the trip wire is relatively large but decreases slowly along the sphere surface (see the r.m.s. velocity profiles at $\phi = 60°$–$90°$ in figure 7*b* and the energy spectra in figure 9*a*). Owing to this disturbance, the mean velocity becomes fuller near the wall than that of smooth sphere, which delays the separation farther downstream. The first separation occurs in between $\phi = 100°$ and 110°. Along the separated shear layer, the r.m.s. velocity fluctuations rapidly increase and the energy at all frequencies increases (figure 9*a*). Then, the mean flow reattaches on the sphere surface in between $\phi = 110°$ and 120°. Hence, a secondary separation bubble is formed on the sphere surface at this Reynolds number (see also figure 5*a*). After reattachment, the main separation is delayed due to high momentum near the wall. As the Reynolds number is increased further, the size of secondary separation bubble decreases and it finally disappears (figure 5*a*). At $Re = 2.3 \times 10^5$ (figure 7*c*), the disturbance induced by the trip wire is very large and decreases only slightly along the downstream direction. The energy spectrum at $\phi = 60°$ is also widebanded as shown in figure 9(*a*), indicating that the boundary layer flow is already turbulent there. Thus, the main separation is delayed to occur at $\phi \approx 120°$.

For the trip wire of $k/d = 1.33 \times 10^{-2}$ located at $\phi = 50°$ (figure 8), it produces very large disturbances to the incoming boundary layer and thus the flow separates at the trip wire and reattaches on the downstream surface at $\phi < 70°$. This separation and reattachment right after the trip wire was already observed from oil-flow patterns in figure 5(*b*). At $Re = 0.5 \times 10^5$ (figure 8*a*), the mean velocity and r.m.s. velocity fluctuation profiles after reattachment do not fully develop to turbulent boundary layer flow (compare these profiles with those for higher Reynolds number cases in figure 8). In other words, the near-wall mean velocity profile is not full enough to

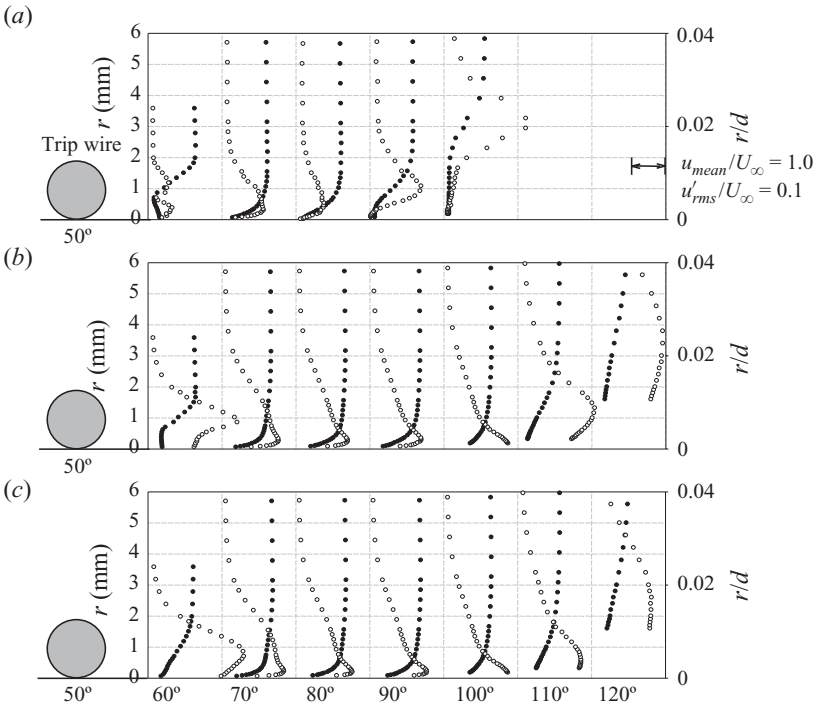

FIGURE 8. Profiles of the mean streamwise velocity (●) and r.m.s. streamwise velocity fluctuations (○) above the sphere surface at $\phi = 60°$–$120°$ for the trip wire of $k/d = 1.33 \times 10^{-2}$ located at $\phi = 50°$: (*a*) $Re = 0.5 \times 10^5$; (*b*) 1.0×10^5; (*c*) 1.5×10^5.

significantly delay the main separation. As a result, the main separation occurs in between $\phi = 80°$–$90°$. The energy spectra at $\phi = 60°$ and $70°$ also show non-turbulent flow characteristics having low energy at high frequencies (figure 9*b*). At $Re = 1.0 \times 10^5$ (figure 8*b*), the flow after reattachment shows turbulent boundary layer characteristics. The energy spectra also show typical broadband characteristics (figure 9*b*). The main separation occurs at $\phi \approx 110°$ without forming secondary separation bubble on the sphere surface, unlike the case of a smaller trip wire. The flow characteristics at $Re = 1.5 \times 10^5$ are similar to those at $Re = 1.0 \times 10^5$, as shown in figure 8(*c*).

3.5. *Mechanism of drag reduction*

In figure 10, we describe the mechanism of drag reduction by the trip wire of $k/d = 0.33 \times 10^{-2}$. At low Reynolds numbers, where the drag reduction does not occur, the disturbance induced by the trip wire decays in the downstream and main separation occurs at a location similar to that of a smooth sphere ($\phi \approx 80°$). At moderate Reynolds numbers, the disturbance from the trip wire also decays along the downstream but is still effective enough to delay the separation. After the first separation, the disturbance rapidly grows from the shear layer instability and the flow reattaches on the sphere surface, forming a secondary separation bubble there. With the increased near-wall momentum, the main separation is significantly delayed. At high Reynolds numbers, the disturbance generated by the trip wire directly induces transition to turbulence inside the boundary layer and turbulent boundary layer flow delays the main separation.

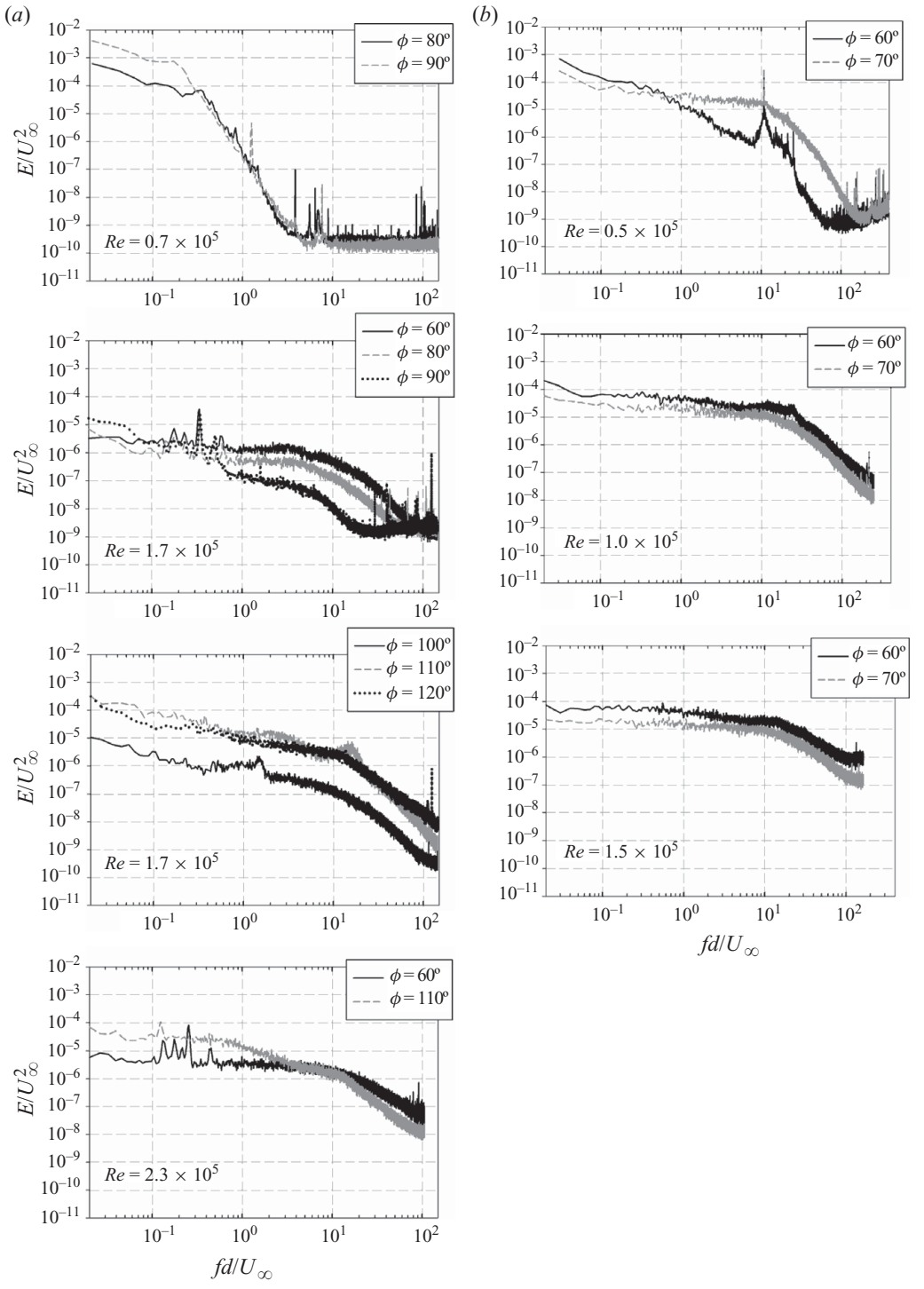

FIGURE 9. Energy spectra of the streamwise velocity at the radial location having maximum u_{rms}: (*a*) $k/d = 0.33 \times 10^{-2}$; (*b*) 1.33×10^{-2}.

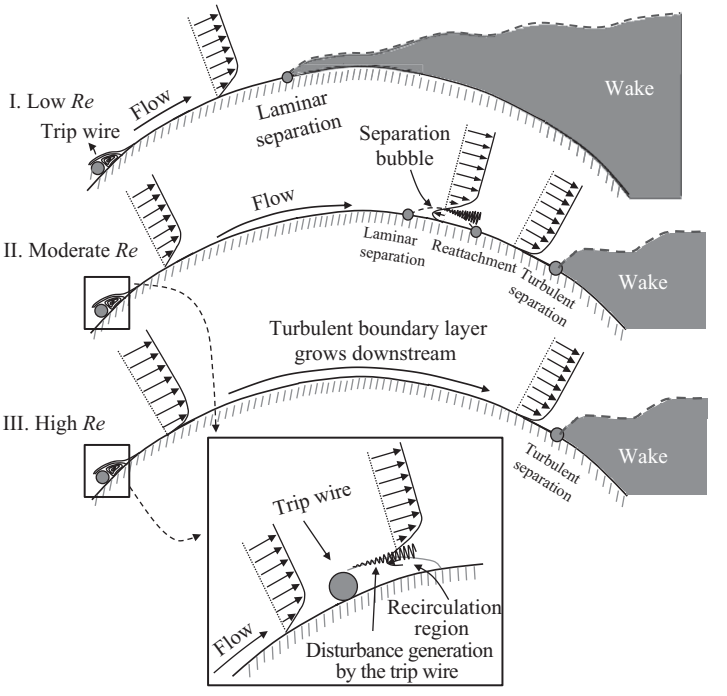

FIGURE 10. Mechanism of drag reduction by the surface trip wire of $k/d = 0.33 \times 10^{-2}$.

When the diameter of the trip wire is much bigger than the local boundary layer thickness (the case of $k/d = 1.33 \times 10^{-2}$), the trip wire itself behaves as an obstacle to the incoming boundary layer. When the Reynolds number is not large enough, the reattached flow behind the trip wire does not bring enough near-wall momentum and drag reduction does not occur. However, at large Reynolds numbers, the reattached flow behind the trip wire becomes fully turbulent flow and delays the main separation, resulting in significant drag reduction (similar to III in figure 10).

4. Summary

In the present study, the characteristics of flow around a sphere with a surface trip wire were experimentally investigated at the subcritical Reynolds numbers of 0.5×10^5–2.8×10^5. A trip wire was placed at various azimuthal locations and the drag of the sphere was measured directly. Measurements of the velocity profiles near the sphere surface were made for two diameters of trip wire. Given the size of the trip wire, the drag coefficient started to decrease at lower Reynolds number for the trip wire located father downstream, but the maximum amount of drag-coefficient decrease (more than 60 %) was nearly insensitive to its azimuthal location. A bigger size of trip wire also reduced the drag coefficient at a lower Reynolds number, but the minimum drag coefficient due to the trip wire was increased slightly more than that of a smaller trip wire.

The primary cause of drag reduction by the trip wire was the delay of main separation on the rear side of the sphere due to the boundary layer becoming turbulent, resulting in a higher pressure recovery. The mechanism leading to this varied with the trip-wire diameter and Reynolds number. We observed three different flow characteristics depending on these parameters. For small values of both parameters,

the disturbance induced by the trip wire decayed downstream and main separation occurred at an azimuthal location similar to that of a smooth sphere. With increasing values of both parameters, the mean velocity after the trip wire became fuller near the wall due to the disturbance from the trip wire and laminar separation was delayed farther downstream. After separation, the transition to turbulence occurred along the separated shear layer, resulting in the flow reattachment to the sphere surface and thus forming a secondary separation bubble on the sphere surface. Then, the main separation was delayed due to high momentum near the surface and the drag was significantly reduced. When the trip wire produced even larger disturbances at the trip-wire location with higher values of both parameters, the boundary layer flow became turbulent already at the front side and the secondary separation bubble was not present.

Promoting transition from laminar to turbulent boundary layer before main separation is critical in drag reduction for a bluff-body flow. We have shown in the present study that there are two ways of promoting transition to turbulence by locating a trip wire on the sphere surface: one by generating a secondary separation bubble at a downstream location of the trip wire, and the other by directly promoting transition to turbulence by forming a relatively large recirculation zone at the trip wire itself. Within the present experimental condition, the first produces slightly more drag reduction than the latter. Therefore, the formation of a secondary separation bubble on a bluff-body surface by appropriately changing the magnitude and/or location of disturbances should be an efficient drag reduction strategy for the control of flow over a bluff body (see also Choi *et al.* 2008).

We acknowledge the financial support from the National Research Laboratory Program (R0A-2006-000-10180-0), World Class University Program (R31-2008-000-10083-0), and Converging Research Center Program (2009-0082824) through the National Research Foundation of Korea funded by the Ministry of Education, Science, and Technology, Korea.

REFERENCES

Achenbach, E. 1972 Experiments on the flow past spheres at very high Reynolds numbers. *J. Fluid Mech.* **54**, 565–575.

Achenbach, E. 1974 The effect of surface roughness and tunnel blockage on the flow past spheres. *J. Fluid Mech.* **65**, 113–125.

Bakić, V. 2004 Experimental investigation of a flow around a sphere. *Therm. Sci.* **8**, 63–81.

Bearman, P. W. & Harvey, J. K. 1976 Golf ball aerodynamics. *Aeronaut. Q.* **27**, 112–122.

Carmichael, B. H. 1981 Low Reynolds number airfoil survey, vol. 1. *NASA Contractor Rep.* 165803.

Choi, H., Jeon, W.-P. & Kim, J. 2008 Control of flow over a bluff body. *Annu. Rev. Fluid Mech.* **40**, 113–139.

Choi, J., Jeon, W.-P. & Choi, H. 2006 Mechanism of drag reduction by dimples on a sphere. *Phys. Fluids* **18**, 041702.

Fage, A. 1936 Experiments on a sphere at critical Reynolds numbers. *Brit. Aero. Res. Counc. Rep. & Mem.* 1766.

Fage, A. & Warsap, G. H. 1929 The effects of turbulence and surface roughness on the drag of a circular cylinder. *Brit. Aero. Res. Counc. Rep. & Mem.* 1283.

Fujita, H., Takahama, H. & Kawai, T. 1985 Effects of tripping wires on heat transfer from a circular cylinder in cross flow. *Bull. Japan. Soc. Mech. Engng* **28**, 80–87.

Gad-el-Hak, M. 1990 Control of low-speed airfoil aerodynamics. *AIAA J.* **28**, 1537–1552.

Gopalarathnam, A., Broughton, B. A., McGranahan, B. D. & Selig, M. S. 2003 Design of low Reynolds number airfoils with trips. *J. Aircraft* **40**, 768–775.

Hover, F. S., Tvedt, H. & Triantafyllou, M. S. 2001 Vortex-induced vibrations of a cylinder with tripping wires. *J. Fluid Mech.* **448**, 175–195.

Igarashi, T. 1986 Effect of tripping wires on the flow around a circular cylinder normal to an airstream. *Bull. Japan. Soc. Mech. Engng* **29**, 2917–2924.

James, D. F. & Truong, Q. S. 1972 Wind load on cylinder with spanwise protrusion. *Proc. ASCE, J. Engng Mech. Div.* **98**, 1573–1589.

Jeon, S., Choi, J., Jeon, W.-P., Choi, H. & Park, J. 2004 Active control of flow over a sphere for drag reduction at a subcritical Reynolds number. *J. Fluid Mech.* **517**, 113–129.

Lissaman, P. B. S. 1983 Low Reynolds number airfoils. *Annu. Rev. Fluid Mech.* **15**, 223–239.

Lyon, C. A., Selig, M. S. & Broeren, A. P. 1997 Boundary layer trips on airfoils at low Reynolds numbers. *AIAA Paper* 97-0511.

Maxworthy, T. 1969 Experiments on the flow around a sphere at high Reynolds numbers. *J. Appl. Mech.* **36**, 598–607.

Moradian, N., Ting, D. S.-K. & Cheng, S. 2009 The effects of freestream turbulence on the drag coefficient of a sphere. *Exp. Therm. Fluid Sci.* **33**, 460–471.

Raithby, G. D. & Eckert, E. R. G. 1968 The effect of support position and turbulence intensity on the flow near the surface of a sphere. *Warme- und Stoffubertragung. Bd.* **1**, 87–94.

Smith, C., Beratlis, N., Balaras, E., Squires, K. & Tsunoda, M. 2009 Numerical investigation of the flow over a golf ball in the subcritical and supercritical regimes. In *Sixth Int. Symp. Turbulence and Shear Flow Phenomena*, pp. 1013–1018.

Son, K., Choi, J., Jeon, W.-P. & Choi, H. 2010 Effect of free-stream turbulence on the flow over a sphere. *Phys. Fluids* **22**, 045101.

Suryanarayana, G. K. & Prabhu, A. 2000 Effect of natural ventilation on the boundary-layer separation and near-wake vortex shedding characteristics of a sphere. *Exp. Fluids* **29**, 582–591.

Torlak, M., Perić, M., Hadžić, I. & Jensen, G. 2004 Numerical simulation of incompressible flow around a sphere with trip wire at $Re = 50\,000$. In *High Performance Computing in Science and Engineering '04*, pp. 189–200. Springer.

Volino, R. J. 2003 Passive flow control on low-pressure turbine airfoils. *ASME J. Turbomach.* **125**, 754–764.

Wieselsberger, C. 1914 A sphere drag (in German). *Zeitschrift für Mechanik* **5**, 140–144.

Zdravkovich, M. M. 1997 *Flow Around Circular Cylinders.* Oxford University Press.

Zhang, X. F. & Hodson, H. 2005 Combined effects of surface trips and unsteady wakes on the boundary layer development of an ultra-high-lift LP turbine blade. *ASME J. Turbomach.* **127**, 479–488.